Published in final edited form as:
Arthritis Rheumatol. 2015 March ; 67(3): 656–667. doi:10.1002/art.38975.

Loss of SH3BP2 function suppresses bone destruction in TNF-driven and collagen-induced arthritis mouse models

Tomoyuki Mukai, MD, PhD[1], **Richard Gallant, BA**[1], **Shu Ishida, DDS**[1,2], **Mizuho Kittaka, DDS, PhD**[1], **Teruhito Yoshitaka, MD, PhD**[1], **David A. Fox, MD**[3], **Yoshitaka Morita, MD, PhD**[4], **Keiichiro Nishida, MD, PhD**[5,6], **Robert Rottapel, MD**[7,8], and **Yasuyoshi Ueki, MD, PhD**[1,*]

[1]Department of Oral and Craniofacial Sciences, School of Dentistry, University of Missouri-Kansas City, Kansas City, MO, USA

[2]Department of Periodontal Medicine, Graduate School of Biomedical Sciences, Hiroshima University, Hiroshima, Japan

[3]Division of Rheumatology, Department of Internal Medicine, University of Michigan, Ann Arbor, MI, USA

[4]Department of Rheumatology, Kawasaki Medical School, Kurashiki, Japan

[5]Department of Orthopaedic Surgery, Okayama University Graduate School of Medicine, Dentistry and Pharmaceutical Sciences, Okayama, Japan

[6]Department of Human Morphology, Okayama University Graduate School of Medicine, Dentistry and Pharmaceutical Sciences, Okayama, Japan

[7]Ontario Cancer Institute and the Campbell Family Cancer Research Institute, University of Toronto, Toronto, Canada

[8]Division of Rheumatology, Department of Medicine, Saint Michael's Hospital, Toronto, Canada

Abstract

Objective—SH3BP2 is a signaling adapter protein which regulates immune and skeletal systems. The purpose of this study was to investigate the role of SH3BP2 in arthritis in human TNF-α transgenic (hTNFtg) and collagen-induced arthritis (CIA) models.

Methods—First, SH3BP2-deficient (*Sh3bp2*$^{-/-}$) and wild-type (*Sh3bp2*$^{+/+}$) mice were crossed with hTNFtg mice. Inflammation and bone loss were examined by clinical inspection and histological and micro-CT analyses. Osteoclastogenesis was evaluated with primary bone marrow-

*Corresponding Author: Yasuyoshi Ueki, MD, PhD Department of Oral and Craniofacial Sciences University of Missouri-Kansas City, School of Dentistry 650 E 25th Street, Kansas City, Missouri 64108, USA uekiy@umkc.edu TEL: +1-816-235-5824 FAX: +1-816-235-5524.

The authors have no conflicting financial interests to declare.

AUTHOR CONTRIBUTIONS

All authors were involved in drafting the article or revising it critically for important intellectual content, and all authors approved the final version to be published. Dr. Ueki had full access to all of the data in the study and takes responsibility for the integrity of the data and the accuracy of the data analysis. Study conception and design. **Mukai, Morita, Nishida, Ueki.**

Acquisition of data. **Mukai, Gallant, Ishida.**

Analysis and interpretation of data. Mukai, Gallant, Ishida, Kittaka, Yoshitaka, Fox, Morita, Nishida, Rottapel, Ueki.

derived M-CSF-dependent macrophages (BMMs). Second, CIA was induced in *Sh3bp2*$^{-/-}$ and *Sh3bp2*$^{+/+}$ mice, and the incidence and severity of arthritis were evaluated. Anti-mouse type II collagen (CII) antibody levels were measured by ELISA. Lymph node cell responses to CII were also determined.

Results—SH3BP2-deficiency did not alter the severity of joint swelling but suppressed bone erosion in the hTNFtg model. Bone loss of talus and tibia was prevented in *Sh3bp2*$^{-/-}$/hTNFtg mice compared to *Sh3bp2*$^{+/+}$/hTNFtg mice. RANKL- and TNF-α-induced osteoclastogenesis was suppressed in *Sh3bp2*$^{-/-}$ BMM cultures. NFATc1 nuclear localization in response to TNF-α was decreased in *Sh3bp2*$^{-/-}$ BMMs compared to *Sh3bp2*$^{+/+}$ BMMs. In the CIA model, SH3BP2-deficiency suppressed the incidence of arthritis, which was associated with decreased anti-CII antibody production, while the antigen-specific T-cell responses in lymph nodes were not significantly different between *Sh3bp2*$^{+/+}$ and *Sh3bp2*$^{-/-}$ mice.

Conclusion—SH3BP2-deficiency prevents bone loss via impaired osteoclastogenesis in the hTNFtg model and suppresses the induction of arthritis via decreased autoantibody production in the CIA model. Therefore, SH3BP2 could be a therapeutic target for rheumatoid arthritis.

Rheumatoid arthritis (RA) is a chronic inflammatory bone destructive disorder with autoimmune features. It is driven by diverse cellular and humoral immune responses, resulting in bone destruction. Bone loss in RA is caused by osteoclasts (1-3). Osteoclast differentiation is controlled mainly by receptor activator of nuclear factor-κB (RANK) and its ligand, RANKL. RANKL is expressed on osteoblasts and can be expressed by other cells such as fibroblasts and T cells in inflammatory conditions (4-6). In RA, tumor necrosis factor (TNF)-α augments RANKL expression in synovial fibroblasts and subsequently enhances osteoclastogenesis in inflamed joints (4-6). Additionally, TNF-α enhances osteoclastogenesis by acting on osteoclast precursors directly or synergistically with RANKL (7-10). Consequently, excessive osteoclast activity causes local and systemic bone loss (11, 12). Additionally, one of the characteristic features of RA is the presence of autoantibodies, notably rheumatoid factor and anti-citrullinated protein antibodies (3, 13). Autoantibody production by B cells is a major pathogenic mechanism leading to chronic inflammation in RA.

SH3 domain-binding protein 2 (SH3BP2) is an adaptor protein, which is expressed primarily in immune cells including T cells, B cells, and macrophages as well as osteoclasts. SH3BP2 interacts with various proteins, including SYK (14), PLCγ (14, 15), and SRC (16, 17), and regulates intracellular signaling pathways in immune and skeletal systems (18-21). Previously we have reported that gain-of-function mutations in SH3BP2 cause a human craniofacial disorder, cherubism (OMIM#118400) (22, 23), characterized by excessive jawbone destruction (24). The cherubism jaw lesions consist mainly of fibroblastoid cells with numerous tartrate-resistant acid phosphatase (TRAP)-positive multinucleated giant cells (24, 25), suggesting that the excessive bone resorption is caused by increased osteoclast formation. We have generated a mouse model of cherubism by knocking-in a P416R SH3BP2 mutation (equivalent to the most common P418R mutation in cherubism patients) (21). Analysis of the mouse model has revealed that heterozygous (*Sh3bp2*$^{P416R/+}$) mice exhibit osteopenia due to increased RANKL-induced osteoclastogenesis (21). Unexpectedly, homozygous mutants (*Sh3bp2*$^{P416R/P416R}$) spontaneously develop severe arthritis. In

SH3BP2-deficient (*Sh3bp2*$^{-/-}$) mice, B-cell proliferation and signaling in response to B-cell antigen receptor (BCR) ligation were impaired, although no noticeable abnormalities in T-cell functions were observed (18, 19). Furthermore, SH3BP2 loss of function suppresses RANKL-induced osteoclastogenesis (16, 17, 26). These findings suggest a potential pathological link between SH3BP2 and arthritis through the SH3BP2 modulation of osteoclastogenesis and autoimmune reactions. However, the exact mechanisms by which SH3BP2 regulates arthritis have not been clarified.

In this study, we hypothesized that SH3BP2 plays a role in the pathogenesis of bone destructive inflammatory diseases such as RA, in which TNF-α and autoantibody production are critically involved (3). To test this hypothesis, we used two different murine arthritis models, a human TNF-α transgenic (hTNFtg) (27, 28) and a collagen-induced arthritis (CIA) model (29, 30). Here we demonstrate that SH3BP2-deficiency prevents bone loss via impaired osteoclastogenesis in the hTNFtg model and suppresses the induction of arthritis via decreased autoantibody production in the CIA model.

MATERIALS AND METHODS

Mice

hTNFtg mice (C57BL/6 background) were obtained from Taconic (Hudson, NY) (27) and crossed with *Sh3bp2*$^{-/-}$ mice (C57BL/6 background) (18) under a crossbreeding agreement. DBA/1J mice were purchased from Jackson Laboratory (Bar Harbor, ME). *Sh3bp2*$^{-/-}$ mice were backcrossed for 10 generations onto the DBA/1 background and used for CIA experiments. All mice were housed in a specific pathogen-free facility. All experimental procedures were approved by the Institutional Animal Care and Use Committees.

Reagents

Recombinant murine M-CSF, RANKL, and TNF-α were obtained from Peprotech (Rocky Hill, NJ). Chick type II collagen (CII), complete Freund's adjuvant (CFA), and anti-mouse CII antibody assay kits were purchased from Chondrex (Redmond, WA).

Evaluation of arthritis in the hTNFtg mice

Arthritis severity of *Sh3bp2*$^{+/+}$/hTNFtg and *Sh3bp2*$^{-/-}$/ hTNFtg mice was assessed once each week until 16 weeks of age in a blinded manner using the criteria as follows: 0 = normal; 1 = mild erythema or swelling of the wrist or ankle or erythema and swelling of 1 digit; 2 = moderate erythema and swelling of the wrist or ankle or more than three inflamed digits; 3 = severe erythema and swelling of the wrist or ankle; 4 = complete erythema and swelling of the wrist and ankle including all digits. Each limb was graded, giving a maximum score of 16. At 16 weeks of age, serum and hindlimbs were collected. Serum concentrations of human and mouse TNF-α were measured with ELISA kits (R&D, Minneapolis, MN). After fixation with 4% paraformaldehyde (PFA) in PBS, hindlimbs were subjected to radiological and histological analyses.

Histological and histomorphometric analysis

Hindlimbs were decalcified in 0.5 M EDTA (pH 7.2) at 4°C for 4 weeks and embedded in paraffin. Sections (6 μm) were stained with hematoxylin and eosin (H&E) and Safranin O. The severities of inflammation and cartilage damage were evaluated in a blinded manner by two independent observers using the criteria: for inflammation, 0 = normal, 1 = mild diffuse inflammatory infiltrates, 2 = moderate inflammatory infiltrates, 3 = marked inflammatory infiltrates, 4 = severe inflammation with pannus formation; for cartilage damage, 0 = normal, 1 = mild loss of Safranin O staining with no obvious chondrocyte loss, 2 = moderate loss of staining with focal mild chondrocyte loss, 3 = marked loss of staining with multifocal marked chondrocyte loss, 4 = severe diffuse loss of staining with multifocal severe chondrocyte loss. TRAP staining counterstained with methyl green was performed to visualize TRAP-positive cells. Histomorphometric measurements were performed using OsteoMeasure software (OsteoMetrics, Atlanta, GA). TRAP-positive multinucleated cells (TRAP+ MNCs) containing 3 or more nuclei were defined as osteoclasts. Eroded surface per bone surface (ES/BS) and number of osteoclasts per bone surface (N.Oc/BS) of talus were determined. The terminology and units were described according to international guidelines (31).

Micro-computed tomographic (micro-CT) analysis

Left hindlimbs were scanned with vivaCT40 (Scanco, Bassersdorf, Switzerland). The threshold was set to 300 for hind paw, 260 for cortical bone of tibia, and 220 for trabecular bone of tibia to distinguish mineralized tissue. The talar bone volume was quantified to evaluate bone erosion (32). The regions of trabecular and cortical bone of tibia were selected as described previously (33). All micro-CT parameters were described according to international guidelines (34).

Osteoclast differentiation assay

Primary bone marrow cell culture was performed as described (21). Mouse bone marrow cells were isolated from long bones of 9-week-old *Sh3bp2*$^{+/+}$ and *Sh3bp2*$^{-/-}$ female mice and cultured on Petri dishes for 2–4 hours. Non-adherent cells were re-seeded on 48-well plates at 2.1×10^4 cells/well and incubated for 2 days in α-MEM/10% FBS containing M-CSF (25 ng/ml) at 37°C/5% CO_2. The bone marrow-derived M-CSF-dependent macrophages (BMMs) were stimulated with RANKL and TNF-α in the presence of M-CSF (25 ng/ml) for additional 4 days. Culture media were changed every other day. TRAP+ MNCs (3 or more nuclei) were visualized by TRAP staining (Sigma-Aldrich, St. Louis, MO) and counted at 40X magnification (n = 4–6 wells/group).

Resorption assay

Dentin slices were sterilized in 70% ethanol, washed with PBS, and placed on the bottom of 96-well plates. Non-adherent bone marrow cells were plated at 8.5×10^3 cells/well. After 2-day preculture with M-CSF, the BMMs were stimulated with RANKL and TNF-α in the presence of M-CSF (25 ng/ml) for 14 days. After removal of the cells with 1M NH_4OH, resorption areas were visualized with toluidine blue, followed by quantification with ImageJ (NIH, Bethesda, MD).

Real-time quantitative PCR (qPCR)

Total RNA was extracted using TRIzol (Invitrogen, Carlsbad, CA). cDNA was transcribed using High Capacity cDNA Reverse Transcription Kits (Applied Biosystems, Carlsbad, CA). qPCR reactions were performed using Absolute Blue QPCR Master Mixes (Thermo Scientific, Waltham, MA) with StepOne Plus system (Applied Biosystems). Gene expression levels relative to *Hprt* were calculated by ΔΔCt method and were normalized to baseline controls. Primers are as follows: *Tnfa*, 5'-catcttctcaaaattcgagtgaca-3' and 5'-tgggagtagacaaggtacaaccc-3'; *Acp5*, 5'-cagcagcccaaaatgcct-3' and 5'-ttttgagccaggacagctga-3'; *Ctsk*, 5'-cgaaaagagcctagcgaaca-3' and 5'-tgggtagcagcagaaacttg-3'; *Oscar*, 5'-tctgccccctatgtgctatca-3' and 5'-aggagccagaaccttcgaaac-3'; *Hprt*, 5'-tcctcctcagaccgctttt-3' and 5'-cctggttcatcatcgctaatc-3'. All qPCR reactions yielded products with single peak dissociation curves.

Western blot

For nuclear and cytoplasmic fractionation, BMMs were lysed on ice in cytoplasmic lysis buffer with protease inhibitors (Sigma-Aldrich), and nuclei were lysed in nuclear lysis buffer as described previously (33). Nuclear (1 μg/lane) and cytoplasmic protein (4 μg/lane) were resolved by SDS-PAGE and transferred to nitrocellulose membranes. After blocking with 5% skim milk, membranes were incubated with primary antibodies followed by incubation with HRP-conjugated secondary antibodies (Cell Signaling Technology). Bands were detected using SuperSignal West chemiluminescent substrates (Thermo Scientific) and visualized by LAS-4000 (GE Healthcare).

Induction of CIA

Nine-week-old *Sh3bp2*$^{+/+}$ and *Sh3bp2*$^{-/-}$ male mice (DBA/1 background) were injected intradermally with 100 μg of chick CII with CFA at the base of the tail on day 0 (35, 36). On day 21, a booster injection was given containing 100 μg of chick CII in incomplete Freund's adjuvant. Arthritis severity was assessed twice each week in a blinded manner until day 70 using the criteria applied for the hTNFtg mice.

ELISA assay for anti-mouse CII antibody

Serum levels of anti-mouse CII antibody (total IgG, IgG1, IgG2a, and IgG2b) were measured according to the manufacturer's protocol. Diluted serum samples were added to mouse CII-coated 96-well plates and incubated at 4°C overnight. Bound IgG was detected by incubation with HRP-conjugated anti-mouse IgG, followed by OPD substrate.

Cell proliferation and cytokine production in draining lymph node cell culture

Nine-week-old *Sh3bp2*$^{+/+}$ and *Sh3bp2*$^{-/-}$ male mice were immunized with 100 μg of chick CII in CFA. At 10 days after the immunization, inguinal lymph nodes were isolated. Lymph node cells were cultured at 4×10^5 cells/well in 96-well U-bottom plates in RPMI1640 with 10% heat-inactivated FBS, 50 μM 2-mercaptoethanol, and 1% L-glutamine at 37°C/5% CO_2 (37). The cells were stimulated with 50 μg/ml of denatured chick CII for 72 hours. Cell proliferation was determined by CellTiter96 Proliferation Assay (MTS) reagent according to

the manufacturer's protocol (Promega, Madison, WI). IFNγ and IL-17 levels in media were determined by ELISA (R&D).

Statistical analysis

All values are given as mean ± SEM. Statistical analysis was performed by the two-tailed unpaired Student's *t*-test to compare two groups and by one-way ANOVA (Tukey-Kramer post-hoc test) to compare three or more groups. Incidence of arthritis was compared by Fisher's exact test. GraphPad Prism 5 (GraphPad, San Diego, CA) was used for all statistical analysis. *P* values less than 0.05 were considered statistically significant.

RESULTS

Suppressed bone erosion in SH3BP2-deficient hTNFtg mice

To investigate the role of SH3BP2 in the pathogenesis of arthritis, we crossed SH3BP2-deficient mice with hTNFtg mice, which spontaneously produce TNF-α and develop TNF-α-dependent arthritis (27, 28). We found that both *Sh3bp2*$^{+/+}$/hTNFtg and *Sh3bp2*$^{-/-}$/hTNFtg mice developed severe arthritis and that the severity of arthritis was comparable between them (Figure 1A). Serum levels of human and murine TNF-α were also similar in *Sh3bp2*$^{+/+}$/hTNFtg and *Sh3bp2*$^{-/-}$/hTNFtg mice (Figure 1B). These data suggest that SH3BP2 deficiency does not significantly affect the severity of joint inflammation and systemic TNF-α production.

Next, we examined the severity of inflammatory cell infiltrates, cartilage damage, and bone erosion in tibio-talar joints. Histological examination showed that both *Sh3bp2*$^{+/+}$/hTNFtg mice and *Sh3bp2*$^{-/-}$/hTNFtg mice developed severe inflammation, but *Sh3bp2*$^{-/-}$/hTNFtg mice exhibited less bone erosive changes (Figure 1C). Quantitative histological analysis revealed that inflammation score and cartilage damage score were comparable between *Sh3bp2*$^{+/+}$/hTNFtg and *Sh3bp2*$^{-/-}$/hTNFtg mice (Figure 1D). Histomorphometric analysis showed that ES/BS and N.Oc/BS were smaller in *Sh3bp2*$^{-/-}$/hTNFtg mice than in *Sh3bp2*$^{+/+}$/hTNFtg mice (Figure 1D). These data suggest that SH3BP2 deficiency suppresses osteoclast formation and bone erosion in inflamed joints without significantly affecting the severity of inflammation.

Decreased focal and systemic bone loss in SH3BP2-deficient hTNFtg mice

Arthritic conditions cause focal bone loss in inflamed joints as well as systemic bone loss (11, 12). To evaluate the focal and systemic bone loss, we analyzed the bone properties of the talus and the tibia as parameters for focal and systemic bone loss, respectively. Micro-CT analysis revealed that both *Sh3bp2*$^{+/+}$/hTNFtg and *Sh3bp2*$^{-/-}$/hTNFtg mice exhibited bone erosion on the talus, but bone erosion was milder in the *Sh3bp2*$^{-/-}$/hTNFtg mice (Figure 2A). To quantify the focal bone loss, the bone volume (BV) of talus and % change of BV of the talus relative to non-inflamed control mice were determined as reported (32). The average BV of the talus in *Sh3bp2*$^{-/-}$/hTNFtg mice was greater than in *Sh3bp2*$^{+/+}$/hTNFtg mice, and the % change of BV of the talus was less in *Sh3bp2*$^{-/-}$/hTNFtg mice (Figure 2B). To examine if SH3BP2 deficiency suppresses systemic bone loss, properties of trabecular and cortical bone of the tibia were determined. We found that bone volume per

total volume (BV/TV) in *Sh3bp2*$^{-/-}$/hTNFtg mice was larger than in *Sh3bp2*$^{+/+}$/hTNFtg mice, and that the rate of trabecular bone loss was smaller in *Sh3bp2*$^{-/-}$/hTNFtg mice than in *Sh3bp2*$^{+/+}$/hTNFtg mice (Figure 2C). Similar findings were observed in cortical thickness (Ct.Th) of the tibia (Figure 2D). In summary, our data show that loss-of-function of SH3BP2 prevents focal and systemic bone loss in the hTNFtg arthritis model.

TNF-α mRNA expression in primary BMMs

We have previously reported that SH3BP2 plays a role in TNF-α production by macrophages as shown by the observation that the P416R SH3BP2 gain-of-function mutation in macrophages resulted in greater TNF-α production in response to M-CSF compared to that of *Sh3bp2*$^{+/+}$ macrophages (21). To examine if SH3BP2 deficiency suppresses TNF-α expression in macrophages, we determined the TNF-α mRNA expression levels in *Sh3bp2*$^{+/+}$ and *Sh3bp2*$^{-/-}$ BMMs in response to M-CSF and TNF-α. M-CSF stimulation did not increase TNF-α mRNA expression during the culture periods (Figure 3A). TNF-α + M-CSF stimulation increased TNF-α mRNA expression by 4-fold at 24 hours after the stimulation, but the expression levels were comparable between *Sh3bp2*$^{+/+}$ and *Sh3bp2*$^{-/-}$ BMMs (Figure 3A). These results suggest that SH3BP2 deficiency does not significantly change the TNF-α expression in BMMs, which is consistent with the result that there is no difference in serum TNF-α levels between *Sh3bp2*$^{+/+}$/hTNFtg and *Sh3bp2*$^{-/-}$/hTNFtg mice (Figure 1B).

Impaired osteoclastogenesis in SH3BP2-deficient primary BMMs

Decreased osteoclasts formation and bone erosion in the inflamed joints of *Sh3bp2*$^{-/-}$ mice led us to investigate the role of SH3BP2 in osteoclastogenesis. Since RANKL and TNF-α are involved in the mechanisms of inflammatory bone resorption (4-6), we examined the role of SH3BP2 in RANKL- and TNF-α-induced osteoclastogenesis. *Sh3bp2*$^{+/+}$ and *Sh3bp2*$^{-/-}$ BMMs were stimulated with RANKL and/or TNF-α in the presence of M-CSF. We found that cell proliferation was comparable between *Sh3bp2*$^{+/+}$ and *Sh3bp2*$^{-/-}$ BMMs after the stimulation (data not shown). RANKL and TNF-α stimulation, respectively, induced TRAP+ MNCs formation in both *Sh3bp2*$^{+/+}$ and *Sh3bp2*$^{-/-}$ BMMs (Figure 3B). *Sh3bp2*$^{-/-}$ BMMs formed less TRAP+ MNCs in response to TNF-α, while the numbers of TRAP+ MNCs were comparable when the BMMs were treated with RANKL and the combination of RANKL and TNF-α (RANKL+TNF-α) (Figure 3B). Consistent with a previous report (16), size of the TRAP+ MNCs from *Sh3bp2*$^{-/-}$ BMMs was smaller than that from *Sh3bp2*$^{+/+}$ BMMs (data not shown). Next, we investigated bone-resorbing function of BMMs after stimulation by RANKL and TNF-α. Although TNF-α alone did not induce detectable resorption pits in *Sh3bp2*$^{+/+}$ BMMs cultures, it enhanced the resorption synergistically with RANKL in *Sh3bp2*$^{+/+}$ osteoclasts (Figure 3C). In contrast, the synergistic induction was much lower in *Sh3bp2*$^{-/-}$ BMMs than that in *Sh3bp2*$^{+/+}$ BMMs.

Taken together, the data demonstrate that SH3BP2 deficiency decreases TRAP+ MNCs formation by TNF-α and inhibits osteoclastic resorbing function in response to RANKL, particularly in the presence of TNF-α, suggesting that loss of SH3BP2 function ameliorates focal and systemic bone loss in the hTNFtg arthritis model by decreasing the formation of functional osteoclasts in response to RANKL and TNF-α.

Decreased NFATc1 nuclear localization in TNF-α-stimulated Sh3bp2$^{-/-}$ BMMs

We next investigated the mechanism by which lack of SH3BP2 impairs RANKL- and TNF-α-induced osteoclastogenesis. Since previous reports have shown that SH3BP2 regulates RANKL-induced osteoclastogenesis via activation of nuclear factor of activated T-cells, cytoplasmic 1 (NFATc1) (17, 21, 26, 38) that is an essential transcription factor for osteoclastogenesis (38, 39), we focused on the NFATc1 levels in BMMs. We found that nuclear expression of NFATc1 was decreased in *Sh3bp2*$^{-/-}$ BMMs at 48 to 72 hours after RANKL, RANKL+TNF-α, and TNF-α stimulation compared to those in *Sh3bp2*$^{+/+}$ BMMs. Particularly, the nuclear NFATc1 expression in *Sh3bp2*$^{-/-}$ BMMs was greatly decreased when BMMs were stimulated with TNF-α alone (Figure 4A). Nuclear expression patterns of other transcription factors such as NF-κB, c-Fos, c-Jun, and IRF8, which also regulate osteoclastogenesis (40, 41), were not different between *Sh3bp2*$^{+/+}$ and *Sh3bp2*$^{-/-}$ BMMs in response to TNF-α (data not shown). These results suggest that decreased NFATc1 nuclear localization in *Sh3bp2*$^{-/-}$ BMMs is, at least in part, responsible for the diminished formation of active osteoclasts in vivo and in vitro.

Since osteoclast-associated genes are primarily regulated by NFATc1 (38), we next examined the mRNA expression of *Acp5*, *Ctsk*, and *Oscar* in *Sh3bp2*$^{+/+}$ and *Sh3bp2*$^{-/-}$ BMMs stimulated with RANKL, RANKL+TNF-α, and TNF-α. We found that expression levels of the genes were reduced in RANKL- and TNF-α-stimulated *Sh3bp2*$^{-/-}$ BMMs compared to those in *Sh3bp2*$^{+/+}$ BMMs (Figure 4B). These findings were similar to the previous findings that reduced function of SH3BP2 suppresses the expression of osteoclast-associated genes in RANKL-induced osteoclastogenesis (17, 26) and support the observation that NFATc1 nuclear localization was decreased in *Sh3bp2*$^{-/-}$ TRAP+ MNCs. However, expression levels of the osteoclast-associated genes were not significantly decreased in response to the simultaneous stimulation with RANKL and TNF-α (Figure 4B), the condition in which *Sh3bp2*$^{-/-}$ TRAP+ MNCs exhibit significantly decreased resorption area (Figure 3C). These findings suggest that SH3BP2 could regulate bone resorption independently of NFATc1 activation, at least, in response to the combination treatment of RANKL and TNF-α.

Lower incidence and severity of arthritis in CII-immunized Sh3bp2$^{-/-}$ mice

SH3BP2 is expressed in various immune cells including T and B cells (18, 19). Next we investigated if SH3BP2 regulates the development of arthritis in a model in which T and B cells play essential roles in the pathogenesis. To this end, we induced CIA in *Sh3bp2*$^{+/+}$ and *Sh3bp2*$^{-/-}$ DBA/1 mice. As shown in Figure 5A, *Sh3bp2*$^{+/+}$ mice developed arthritis at a rate of 100% (10 out of 10 mice), while the induction of arthritis in *Sh3bp2*$^{-/-}$ mice was significantly suppressed (15%, 2 out of 13 mice). Additionally, the severity of arthritis in *Sh3bp2*$^{-/-}$ mice was much lower than that of *Sh3bp2*$^{+/+}$ mice (Figure 5B). These data indicate that SH3BP2 deficiency suppresses the development of arthritis in the CIA model.

Decreased inflammation and cartilage damage in joints of Sh3bp2$^{-/-}$ mice

To determine the effect of SH3BP2 deficiency on inflammation, cartilage damage, and bone erosion in the CIA model, histological analysis was performed on the ankle joints of CII-immunized *Sh3bp2*$^{+/+}$ (n = 10) and *Sh3bp2*$^{-/-}$ (n = 13) mice as well as their non-

immunized *Sh3bp2*$^{+/+}$ (*n* = 7) and *Sh3bp2*$^{-/-}$ (*n* = 7) controls. We found that CII-immunized *Sh3bp2*$^{+/+}$ mice developed severe inflammation, cartilage damage, and bone erosion with osteoclast formation, while CII-immunized *Sh3bp2*$^{-/-}$ mice developed much milder inflammation, cartilage damage, and bone erosion with decreased osteoclast formation compared with CII-immunized *Sh3bp2*$^{+/+}$ mice (Figure 5C). The findings were confirmed by quantitative analysis of inflammation and cartilage damage and by histomorphometric analysis (Figure 5D). These data indicate that the SH3BP2 deficiency decreases the severity of inflammation, cartilage damage, and bone erosion, reflecting decreased joint inflammation and osteoclast formation in *Sh3bp2*$^{-/-}$ mice.

Suppressed serum anti-mouse CII antibody levels in Sh3bp2$^{-/-}$ mice

To dissect the mechanisms underlying the suppressed induction of arthritis in *Sh3bp2*$^{-/-}$ mice in the CIA model, we determined the serum levels of autoantibody, which is important for the induction of CIA (29, 30). As shown in Figure 6A, total IgG levels against mouse CII at day 70 were increased in CII-immunized *Sh3bp2*$^{+/+}$ mice, while SH3BP2 deficiency dramatically suppressed the serum levels of the antibody. IgG1, IgG2a, IgG2b subclasses of anti-CII antibody were all decreased in CII-immunized *Sh3bp2*$^{-/-}$ mice compared with CII-immunized *Sh3bp2*$^{+/+}$ mice (Figure 6A). These results indicate that suppressed induction of arthritis in *Sh3bp2*$^{-/-}$ mice is associated with decreased anti-mouse CII antibody production.

No significant abnormality in proliferation and IFNγ and IL-17 production in Sh3bp2$^{-/-}$ draining lymph node cell culture

T cells also play critical roles in the initiation of arthritis in the CIA model (29, 30). To evaluate if impaired T-cell function is involved in the decreased CIA development in *Sh3bp2*$^{-/-}$ mice, inguinal lymph nodes were isolated at 10 days after the CII immunization. Proliferation of the cells and levels of IFNγ and IL-17 production in response to chick CII were determined. We found that the cell proliferation and the cytokine levels in the media were comparable between the CII-immunized *Sh3bp2*$^{+/+}$ and *Sh3bp2*$^{-/-}$ cells (Figure 6B–C). These results suggest that SH3BP2 deficiency does not significantly alter the pathogenic T-cell responses in CIA, in contrast to impaired production of the associated autoantibodies.

DISCUSSION

Previous studies on SH3BP2-deficient mice have shown that, in physiological conditions, SH3BP2 is important for RANKL-induced osteoclastic bone resorption (16). In this study, we demonstrated that the lack of SH3BP2 suppresses inflammatory bone destruction using two different arthritis models, hTNFtg mice and CIA.

Accumulating evidence suggests that RANKL and TNF-α play important roles in inflammatory bone destructive diseases such as RA (4-6). We hypothesized that SH3BP2 contributes to RANKL- and TNF-α-induced osteoclastogenesis in pathological inflammatory conditions, and obtained several pieces of evidence to support this hypothesis. First, loss-of-function of SH3BP2 ameliorated inflammatory bone destruction in hTNFtg mice associated with reduced numbers of TRAP+ MNCs. Second, RANKL- and TNF-α-

induced osteoclastogenesis was impaired in SH3BP2-deficient BMMs. Third, NFATc1 induction and expression of osteoclast-associated genes (*Acp5*, *Cathepsin K*, and *Oscar*) were reduced in *Sh3bp2*$^{-/-}$ BMMs in response to TNF-α. In addition to its direct effect on TRAP+ MNC formation, TNF-α potentiates functional osteoclast formation synergistically with RANKL (7, 9, 10). Based on these results, we conclude that SH3BP2 plays an important role in both RANKL- and TNF-α-induced osteoclastogenesis and regulates bone destruction in pathological inflammatory conditions through modulating the responsiveness to RANKL and TNF-α.

Consistent with the previous report (16), we showed that SH3BP2 deficiency suppresses RANKL-induced osteoclastic bone resorption, but not TRAP+ MNC formation (Figure 3B, C). Interestingly, our study also revealed that SH3BP2 deficiency suppresses the TRAP+ MNC formation in response to TNF-α (Figure 3B), suggesting that the mechanism by which SH3BP2 regulates osteoclastogenesis differs between RANKL and TNF-α stimulation. In fact, the involvement of NFATc1 is different. Levaot et al. reported that SH3BP2 deficiency does not alter the levels of NFATc1 nuclear localization in RANKL-stimulated BMMs (16), while we found decreased NFATc1 nuclear localization in TNF-α-stimulated *Sh3bp2*$^{-/-}$ BMMs. These findings suggest that in osteoclast precursors SH3BP2 modulates multiple pathways depending on the type of stimulation, presumably by interacting with different signaling molecules. Indeed, several differences have been reported in the regulatory mechanisms between RANKL- and TNF-α-induced osteoclastogenesis (41, 42). We showed that SH3BP2 deficiency dramatically suppresses resorption area in response to RANKL +TNF-α (Figure 3C), but exhibits a relatively small suppressive effect on nuclear NFATc1 localization in response to RANKL+TNF-α (Figure 4A). These findings raise a possibility that SH3BP2 could regulate bone resorption independently of NFATc1-mediated pathways. Further study would be required to test this hypothesis.

Blocking of SH3BP2 function may provide another benefit for the treatment of autoimmune inflammatory diseases. In the present study, we found that SH3BP2 deficiency suppresses the induction of CIA associated with decreased autoantibody production, while T-cell responses against CII are not significantly affected. These results are supported by previous reports demonstrating essential roles of SH3BP2 in B-cell activation. SH3BP2 is shown to be required for optimal B-cell responses without noticeably affecting T-cell function in *Sh3bp2*$^{-/-}$ mice (18, 19). In B cells, SH3BP2 regulates cell proliferation, cell cycle progression, and intracellular signaling pathways downstream of BCR. Intriguingly, SH3BP2 activates NFAT in B cell through the similar mechanisms that SH3BP2 employs in osteoclasts (43, 44). Considering the fact that SH3BP2-deficiency decreases pathogenic autoantibody production in the CIA model, therapeutic strategies designed to suppress SH3BP2 function may be effective for antibody-induced diseases such as systemic lupus erythematosus or refractory immune thrombocytopenia.

Other than monocyte lineage cells and B cells, SH3BP2 plays functional roles in various immune cells including NK cells, neutrophils, and mast cells (15, 45, 46). Given the fact that these cells are also involved in the pathogenesis of RA (3, 47-49), SH3BP2 might contribute to the development of the disease through its roles on the immune cells. Additionally, we cannot exclude the possibility that SH3BP2 regulates osteoclastogenesis indirectly via

osteoblasts and synovial fibroblasts in vivo (50). To achieve better understanding of SH3BP2 function, in vitro analysis with specific cell types isolated from SH3BP2-deficient mice and analysis of SH3BP2 conditional knockout mice or bone marrow chimera models between SH3BP2-deficient and wild-type mice would be beneficial.

In conclusion, we demonstrate that lack of SH3BP2 decreases inflammatory bone loss via impaired osteoclastogenesis in the hTNFtg arthritis model and that SH3BP2 deficiency suppresses induction of arthritis via decreased autoantibody production in the CIA model. These findings suggest that SH3BP2 could be a potential therapeutic target for RA. Although a direct association between SH3BP2 and RA has not yet been identified, genetic variations that affect the expression or functional level of SH3BP2 may regulate the susceptibility and severity of RA, especially through the mechanisms that control autoantibody production by B cells and bone loss by osteoclasts. Further analysis would be required to determine whether activation of SH3BP2-mediated pathways in B cells and osteoclast precursors are involved in the autoimmune and bone destructive features of human diseases.

ACKNOWLEDGMENTS

We would like to thank Drs. Lynda Bonewald, Mark Johnson, Jeffrey Gorski, and Sarah Dallas and all members of Bone Biology Research Program in the Department of Oral and Craniofacial Sciences at University of Missouri-Kansas City (UMKC), School of Dentistry for critical discussion and helpful suggestions. We appreciate Yixia Xie and Mark Dallas for their technical assistance. We are also indebted to the staff at the UMKC Laboratory Animal Research Core for their animal care.

This study was supported by grants from the National Institute of Health (R01DE020835) to Dr. Ueki, the Japan Rheumatism Foundation (Rheumatology Traveling Fellowship) to Dr. Mukai, Research Project Grants from Kawasaki Medical School (No. 26-75) to Dr. Morita, and the Canadian Institute for Health Research CIHR to Dr. Rottapel.

REFERENCES

1. Pettit AR, Ji H, von Stechow D, Muller R, Goldring SR, Choi Y, et al. TRANCE/RANKL knockout mice are protected from bone erosion in a serum transfer model of arthritis. The American journal of pathology. 2001; 159(5):1689–99. [PubMed: 11696430]
2. Redlich K, Hayer S, Ricci R, David JP, Tohidast-Akrad M, Kollias G, et al. Osteoclasts are essential for TNF-alpha-mediated joint destruction. J Clin Invest. 2002; 110(10):1419–27. [PubMed: 12438440]
3. McInnes IB, Schett G. The pathogenesis of rheumatoid arthritis. The New England journal of medicine. 2011; 365(23):2205–19. [PubMed: 22150039]
4. Redlich K, Smolen JS. Inflammatory bone loss: pathogenesis and therapeutic intervention. Nature reviews Drug discovery. 2012; 11(3):234–50.
5. Schett G, Gravallese E. Bone erosion in rheumatoid arthritis: mechanisms, diagnosis and treatment. Nature reviews Rheumatology. 2012; 8(11):656–64.
6. Takayanagi H. New developments in osteoimmunology. Nature reviews Rheumatology. 2012; 8(11):684–9.
7. Lam J, Takeshita S, Barker JE, Kanagawa O, Ross FP, Teitelbaum SL. TNF-alpha induces osteoclastogenesis by direct stimulation of macrophages exposed to permissive levels of RANK ligand. J Clin Invest. 2000; 106(12):1481–8. [PubMed: 11120755]
8. D OG, Ireland D, Bord S, Compston JE. Joint erosion in rheumatoid arthritis: interactions between tumour necrosis factor alpha, interleukin 1, and receptor activator of nuclear factor kappaB ligand (RANKL) regulate osteoclasts. Ann Rheum Dis. 2004; 63(4):354–9. [PubMed: 15020327]

9. Fuller K, Murphy C, Kirstein B, Fox SW, Chambers TJ. TNFalpha potently activates osteoclasts, through a direct action independent of and strongly synergistic with RANKL. Endocrinology. 2002; 143(3):1108–18. [PubMed: 11861538]
10. Kobayashi K, Takahashi N, Jimi E, Udagawa N, Takami M, Kotake S, et al. Tumor necrosis factor alpha stimulates osteoclast differentiation by a mechanism independent of the ODF/RANKL-RANK interaction. The Journal of experimental medicine. 2000; 191(2):275–86. [PubMed: 10637272]
11. Geusens P, Lems WF. Osteoimmunology and osteoporosis. Arthritis Res Ther. 2011; 13(5):242. [PubMed: 21996023]
12. Gough AK, Lilley J, Eyre S, Holder RL, Emery P. Generalised bone loss in patients with early rheumatoid arthritis. Lancet. 1994; 344(8914):23–7. [PubMed: 7912297]
13. Vander Cruyssen B, Peene I, Cantaert T, Hoffman IE, De Rycke L, Veys EM, et al. Anti-citrullinated protein/peptide antibodies (ACPA) in rheumatoid arthritis: specificity and relation with rheumatoid factor. Autoimmunity reviews. 2005; 4(7):468–74. [PubMed: 16137613]
14. Deckert M, Tartare-Deckert S, Hernandez J, Rottapel R, Altman A. Adaptor function for the Syk kinases-interacting protein 3BP2 in IL-2 gene activation. Immunity. 1998; 9(5):595–605. [PubMed: 9846481]
15. Jevremovic D, Billadeau DD, Schoon RA, Dick CJ, Leibson PJ. Regulation of NK cell-mediated cytotoxicity by the adaptor protein 3BP2. J Immunol. 2001; 166(12):7219–28. [PubMed: 11390470]
16. Levaot N, Simoncic PD, Dimitriou ID, Scotter A, La Rose J, Ng AH, et al. 3BP2-deficient mice are osteoporotic with impaired osteoblast and osteoclast functions. J Clin Invest. 2011; 121(8): 3244–57. [PubMed: 21765218]
17. GuezGuez A, Prod'homme V, Mouska X, Baudot A, Blin-Wakkach C, Rottapel R, et al. 3BP2 adapter protein is required for receptor activator of NFkappaB ligand (RANKL)-induced osteoclast differentiation of RAW264.7 cells. The Journal of biological chemistry. 2010; 285(27): 20952–63. [PubMed: 20439986]
18. Chen G, Dimitriou ID, La Rose J, Ilangumaran S, Yeh WC, Doody G, et al. The 3BP2 adapter protein is required for optimal B-cell activation and thymus-independent type 2 humoral response. Molecular and cellular biology. 2007; 27(8):3109–22. [PubMed: 17283041]
19. de la Fuente MA, Kumar L, Lu B, Geha RS. 3BP2 deficiency impairs the response of B cells, but not T cells, to antigen receptor ligation. Molecular and cellular biology. 2006; 26(14):5214–25. [PubMed: 16809760]
20. Sada K, Miah SM, Maeno K, Kyo S, Qu X, Yamamura H. Regulation of FcepsilonRI-mediated degranulation by an adaptor protein 3BP2 in rat basophilic leukemia RBL-2H3 cells. Blood. 2002; 100(6):2138–44. [PubMed: 12200378]
21. Ueki Y, Lin CY, Senoo M, Ebihara T, Agata N, Onji M, et al. Increased myeloid cell responses to M-CSF and RANKL cause bone loss and inflammation in SH3BP2 “cherubism” mice. Cell. 2007; 128(1):71–83. [PubMed: 17218256]
22. Tiziani V, Reichenberger E, Buzzo CL, Niazi S, Fukai N, Stiller M, et al. The gene for cherubism maps to chromosome 4p16. American journal of human genetics. 1999; 65(1):158–66. [PubMed: 10364528]
23. Ueki Y, Tiziani V, Santanna C, Fukai N, Maulik C, Garfinkle J, et al. Mutations in the gene encoding c-Abl-binding protein SH3BP2 cause cherubism. Nat Genet. 2001; 28(2):125–6. [PubMed: 11381256]
24. Papadaki ME, Lietman SA, Levine MA, Olsen BR, Kaban LB, Reichenberger EJ. Cherubism: best clinical practice. Orphanet J Rare Dis. 2012; 7(Suppl 1):S6. [PubMed: 22640403]
25. Southgate J, Sarma U, Townend JV, Barron J, Flanagan AM. Study of the cell biology and biochemistry of cherubism. Journal of clinical pathology. 1998; 51(11):831–7. [PubMed: 10193324]
26. Kawamoto T, Fan C, Gaivin RJ, Levine MA, Lietman SA. Decreased SH3BP2 inhibits osteoclast differentiation and function. Journal of orthopaedic research : official publication of the Orthopaedic Research Society. 2011; 29(10):1521–7. [PubMed: 21448930]

27. Hayward MD, Jones BK, Saparov A, Hain HS, Trillat AC, Bunzel MM, et al. An extensive phenotypic characterization of the hTNFalpha transgenic mice. BMC physiology. 2007; 7:13. [PubMed: 18070349]

28. Keffer J, Probert L, Cazlaris H, Georgopoulos S, Kaslaris E, Kioussis D, et al. Transgenic mice expressing human tumour necrosis factor: a predictive genetic model of arthritis. The EMBO journal. 1991; 10(13):4025–31. [PubMed: 1721867]

29. Seki N, Sudo Y, Yoshioka T, Sugihara S, Fujitsu T, Sakuma S, et al. Type II collagen-induced murine arthritis. I. Induction and perpetuation of arthritis require synergy between humoral and cell-mediated immunity. J Immunol. 1988; 140(5):1477–84. [PubMed: 3257978]

30. Cho YG, Cho ML, Min SY, Kim HY. Type II collagen autoimmunity in a mouse model of human rheumatoid arthritis. Autoimmunity reviews. 2007; 7(1):65–70. [PubMed: 17967728]

31. Dempster DW, Compston JE, Drezner MK, Glorieux FH, Kanis JA, Malluche H, et al. Standardized nomenclature, symbols, and units for bone histomorphometry: a 2012 update of the report of the ASBMR Histomorphometry Nomenclature Committee. Journal of bone and mineral research : the official journal of the American Society for Bone and Mineral Research. 2013; 28(1):2–17.

32. Proulx ST, Kwok E, You Z, Papuga MO, Beck CA, Shealy DJ, et al. Longitudinal assessment of synovial, lymph node, and bone volumes in inflammatory arthritis in mice by in vivo magnetic resonance imaging and microfocal computed tomography. Arthritis Rheum. 2007; 56(12):4024–37. [PubMed: 18050199]

33. Mukai T, Ishida S, Ishikawa R, Yoshitaka T, Kittaka M, Gallant R, et al. SH3BP2 Cherubism Mutation Potentiates TNF-alpha-Induced Osteoclastogenesis Via NFATc1 and TNF-alpha-Mediated Inflammatory Bone Loss. Journal of bone and mineral research : the official journal of the American Society for Bone and Mineral Research. 2014

34. Bouxsein ML, Boyd SK, Christiansen BA, Guldberg RE, Jepsen KJ, Muller R. Guidelines for assessment of bone microstructure in rodents using micro-computed tomography. Journal of bone and mineral research : the official journal of the American Society for Bone and Mineral Research. 2010; 25(7):1468–86.

35. Morita Y, Yang J, Gupta R, Shimizu K, Shelden EA, Endres J, et al. Dendritic cells genetically engineered to express IL-4 inhibit murine collagen-induced arthritis. J Clin Invest. 2001; 107(10): 1275–84. [PubMed: 11375417]

36. Brand DD, Latham KA, Rosloniec EF. Collagen-induced arthritis. Nature protocols. 2007; 2(5): 1269–75.

37. Inglis JJ, Simelyte E, McCann FE, Criado G, Williams RO. Protocol for the induction of arthritis in C57BL/6 mice. Nature protocols. 2008; 3(4):612–8.

38. Aliprantis AO, Ueki Y, Sulyanto R, Park A, Sigrist KS, Sharma SM, et al. NFATc1 in mice represses osteoprotegerin during osteoclastogenesis and dissociates systemic osteopenia from inflammation in cherubism. J Clin Invest. 2008; 118(11):3775–89. [PubMed: 18846253]

39. Takayanagi H, Kim S, Koga T, Nishina H, Isshiki M, Yoshida H, et al. Induction and activation of the transcription factor NFATc1 (NFAT2) integrate RANKL signaling in terminal differentiation of osteoclasts. Developmental cell. 2002; 3(6):889–901. [PubMed: 12479813]

40. Zhao B, Takami M, Yamada A, Wang X, Koga T, Hu X, et al. Interferon regulatory factor-8 regulates bone metabolism by suppressing osteoclastogenesis. Nature medicine. 2009; 15(9): 1066–71.

41. Yao Z, Xing L, Boyce BF. NF-kappaB p100 limits TNF-induced bone resorption in mice by a TRAF3-dependent mechanism. J Clin Invest. 2009; 119(10):3024–34. [PubMed: 19770515]

42. Zhao B, Grimes SN, Li S, Hu X, Ivashkiv LB. TNF-induced osteoclastogenesis and inflammatory bone resorption are inhibited by transcription factor RBP-J. The Journal of experimental medicine. 2012; 209(2):319–34. [PubMed: 22249448]

43. Foucault I, Le Bras S, Charvet C, Moon C, Altman A, Deckert M. The adaptor protein 3BP2 associates with VAV guanine nucleotide exchange factors to regulate NFAT activation by the B-cell antigen receptor. Blood. 2005; 105(3):1106–13. [PubMed: 15345594]

44. Shukla U, Hatani T, Nakashima K, Ogi K, Sada K. Tyrosine phosphorylation of 3BP2 regulates B cell receptor-mediated activation of NFAT. J Biol Chem. 2009; 284(49):33719–28. [PubMed: 19833725]
45. Chen G, Dimitriou I, Milne L, Lang KS, Lang PA, Fine N, et al. The 3BP2 adapter protein is required for chemoattractant-mediated neutrophil activation. Journal of immunology. 2012; 189(5):2138–50.
46. Ainsua-Enrich E, Alvarez-Errico D, Gilfillan AM, Picado C, Sayos J, Rivera J, et al. The adaptor 3BP2 is required for early and late events in FcepsilonRI signaling in human mast cells. J Immunol. 2012; 189(6):2727–34. [PubMed: 22896635]
47. Hendrich C, Kuipers JG, Kolanus W, Hammer M, Schmidt RE. Activation of CD16+ effector cells by rheumatoid factor complex. Role of natural killer cells in rheumatoid arthritis. Arthritis Rheum. 1991; 34(4):423–31. [PubMed: 1707275]
48. Cross A, Bucknall RC, Cassatella MA, Edwards SW, Moots RJ. Synovial fluid neutrophils transcribe and express class II major histocompatibility complex molecules in rheumatoid arthritis. Arthritis Rheum. 2003; 48(10):2796–806. [PubMed: 14558085]
49. Malone DG, Wilder RL, Saavedra-Delgado AM, Metcalfe DD. Mast cell numbers in rheumatoid synovial tissues. Correlations with quantitative measures of lymphocytic infiltration and modulation by antiinflammatory therapy. Arthritis Rheum. 1987; 30(2):130–7. [PubMed: 3548731]
50. Wang CJ, Chen IP, Koczon-Jaremko B, Boskey AL, Ueki Y, Kuhn L, et al. Pro416Arg cherubism mutation in Sh3bp2 knock-in mice affects osteoblasts and alters bone mineral and matrix properties. Bone. 2010; 46(5):1306–15. [PubMed: 20117257]

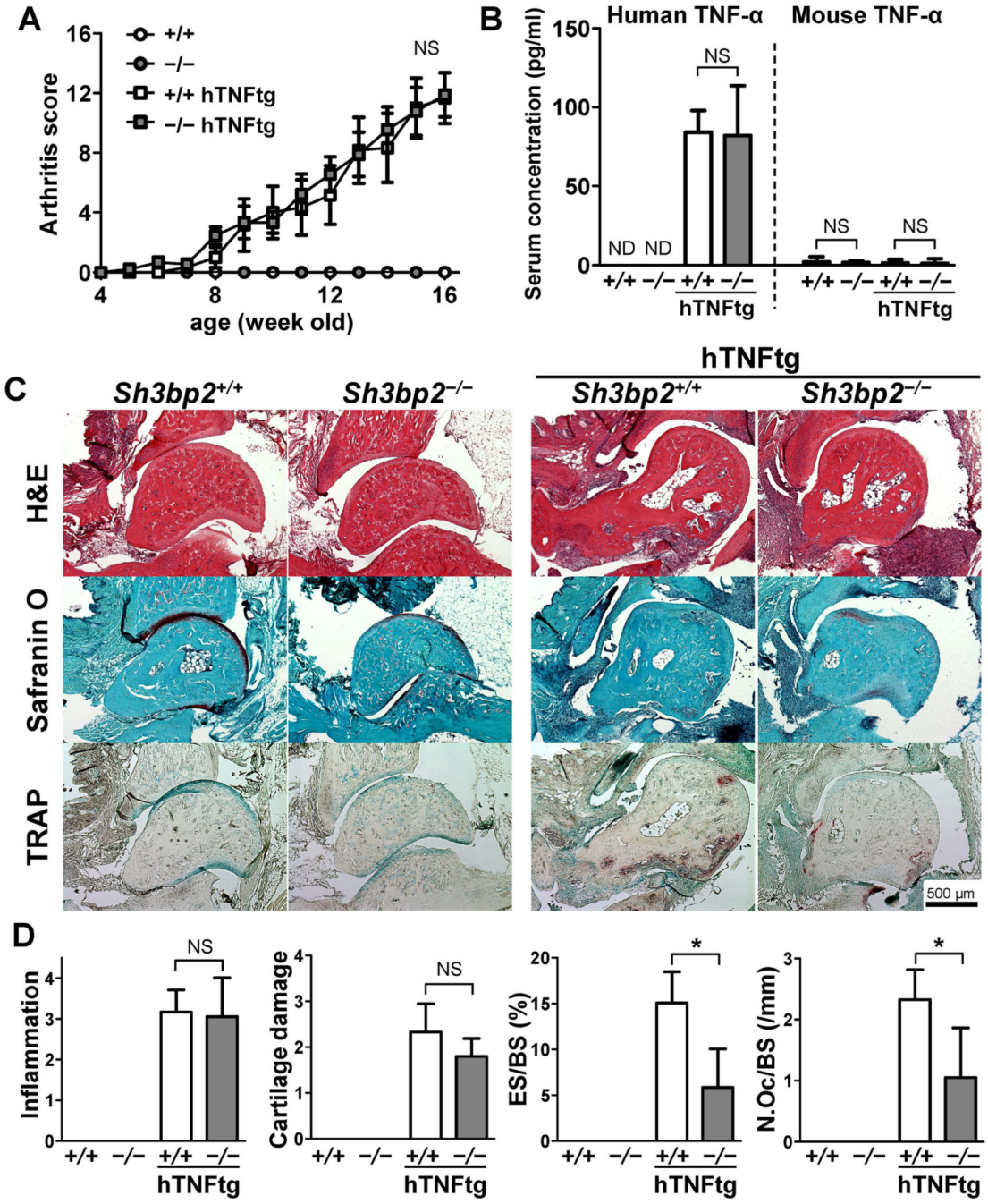

Figure 1.

Decreased osteoclast formation and bone erosion in SH3BP2-deficient human TNF-α-transgenic mice. Sh3bp2$^{+/+}$ and *Sh3bp2*$^{-/-}$ mice were crossed with human TNF-α transgenic (hTNFtg) mice. Joint inflammation was monitored until the age of 16 weeks. Serum and hindlimbs were collected and subjected to ELISA and histological analysis, respectively. **A**, Changes in clinically assessed joint inflammation scores in the *Sh3bp2*$^{+/+}$ (n = 9), *Sh3bp2*$^{-/-}$ (n = 7), *Sh3bp2*$^{+/+}$/hTNFtg (n = 7), and *Sh3bp2*$^{-/-}$/hTNFtg (n = 9) male mice. **B**, Serum concentrations of human and mouse TNF-α. **C**, Representative staining

images of the ankle joint tissues. Ankle joint sections were stained with hematoxylin and eosin (H&E), Safranin O, and tartrate-resistant acid phosphatase (TRAP). Original magnification: 40X. **D**, Histological scores of inflammation and cartilage damage and histomorphometric analysis of talar bones. Bone erosion on the surface of the talus was traced, and attached osteoclasts were counted. Eroded surface per bone surface (ES/BS) and number of osteoclast per bone surface (N.Oc/BS) of the talus were determined. Values are presented as the mean ± SEM. +/+ = *Sh3bp2*$^{+/+}$; −/− = *Sh3bp2*$^{-/-}$. * = $P < 0.05$; NS = not significant; ND = not detectable.

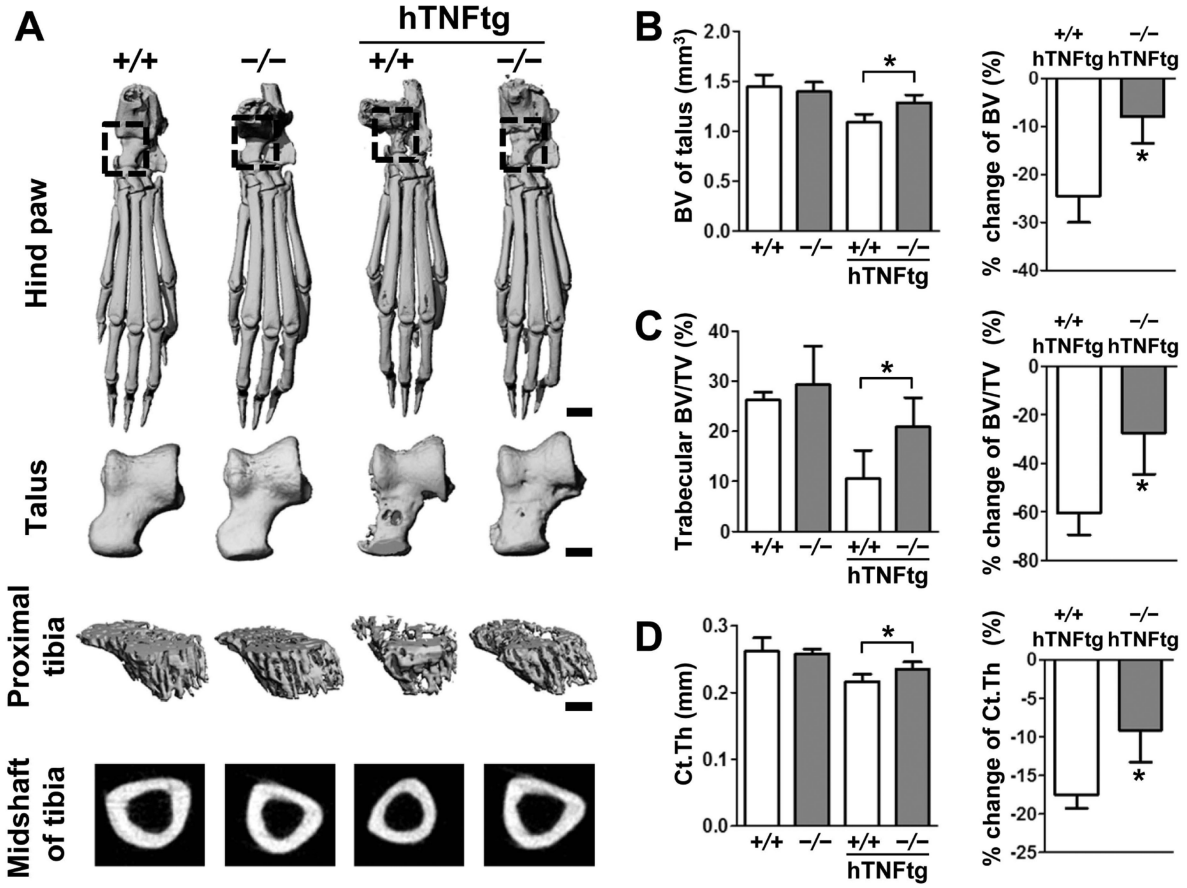

Figure 2.

Decreased focal and systemic bone loss in SH3BP2-deficient human TNF-α-transgenic mice. Left hindlimbs were collected from 16-week-old *Sh3bp2*$^{+/+}$ (*n* = 9), *Sh3bp2*$^{-/-}$ (*n* = 7), *Sh3bp2*$^{+/+}$/hTNFtg (*n* = 7), and *Sh3bp2*$^{-/-}$/hTNFtg (*n* = 9) male mice. The hind paws and tibiae were analyzed with micro-CT. **A**, Representative micro-CT images of hind paws, talar bones, and trabecular and cortical bones of tibiae. Scale bars: 1 mm for hind paw and 400 μm for talus and tibia. **B**, Bone volume (BV) of talus and % change of the BV. % change was calculated relative to *Sh3bp2*$^{+/+}$ and *Sh3bp2*$^{-/-}$ control mice. **C**, Bone volume per total volume (BV/TV) in trabecular bone of proximal tibia and % change of the trabecular BV/TV. **D**, Cortical thickness (Ct.Th) of midshaft of tibia and % change of the Ct.Th. Values are presented as the mean ± SEM. +/+ = *Sh3bp2*$^{+/+}$; −/− = *Sh3bp2*$^{-/-}$. * = $P < 0.05$.

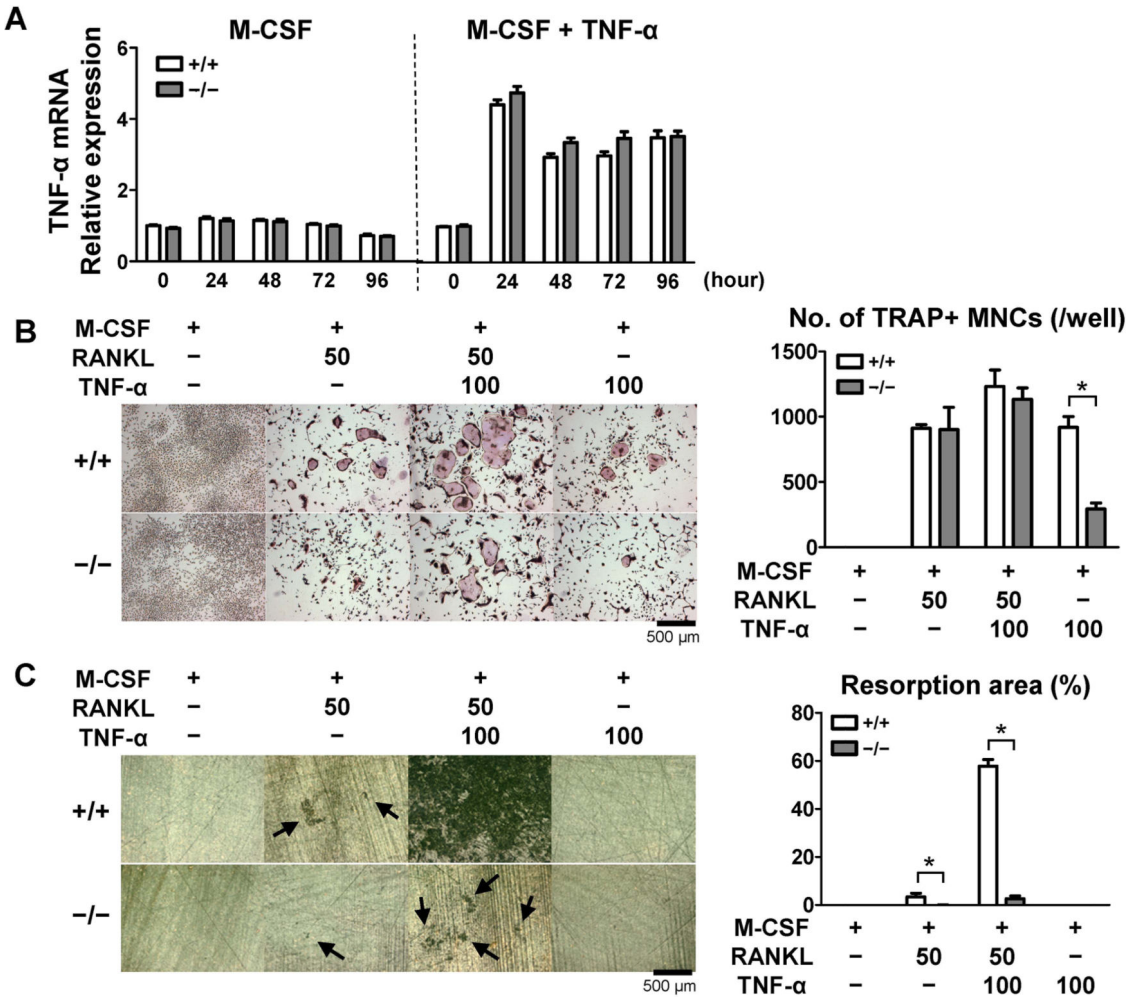

Figure 3.

Impaired osteoclast differentiation and bone-resorbing function in Sh3bp2$^{-/-}$ bone marrow-derived macrophages. Primary bone marrow cells were isolated and cultured as described in Methods section. **A**, TNF-α mRNA expression. Bone marrow-derived macrophages (BMMs) were stimulated with TNF-α (100 ng/ml) in the presence of M-CSF (25 ng/ml). TNF-α mRNA expression levels relative to *Hprt* were calculated and normalized to the expression level of *Sh3bp2*$^{+/+}$ BMMs at 0 hour. **B**, Representative TRAP staining images and number of TRAP-positive multinucleated cells (TRAP+ MNCs). BMMs were stimulated with RANKL (50 ng/ml) and/or TNF-α (100 ng/ml) in the presence of M-CSF (25 ng/ml) for 4 days. Original magnification: 40X. **C**, Representative images and quantification of resorption area on dentine. BMMs were stimulated with RANKL (50 ng/ml) and/or TNF-α (100 ng/ml) in the presence of M-CSF (25 ng/ml) for 14 days. After removal of the cells, resorption areas were visualized by toluidine blue. Original magnification: 50X. Percentages of the resorption areas relative to total surface area were quantified.

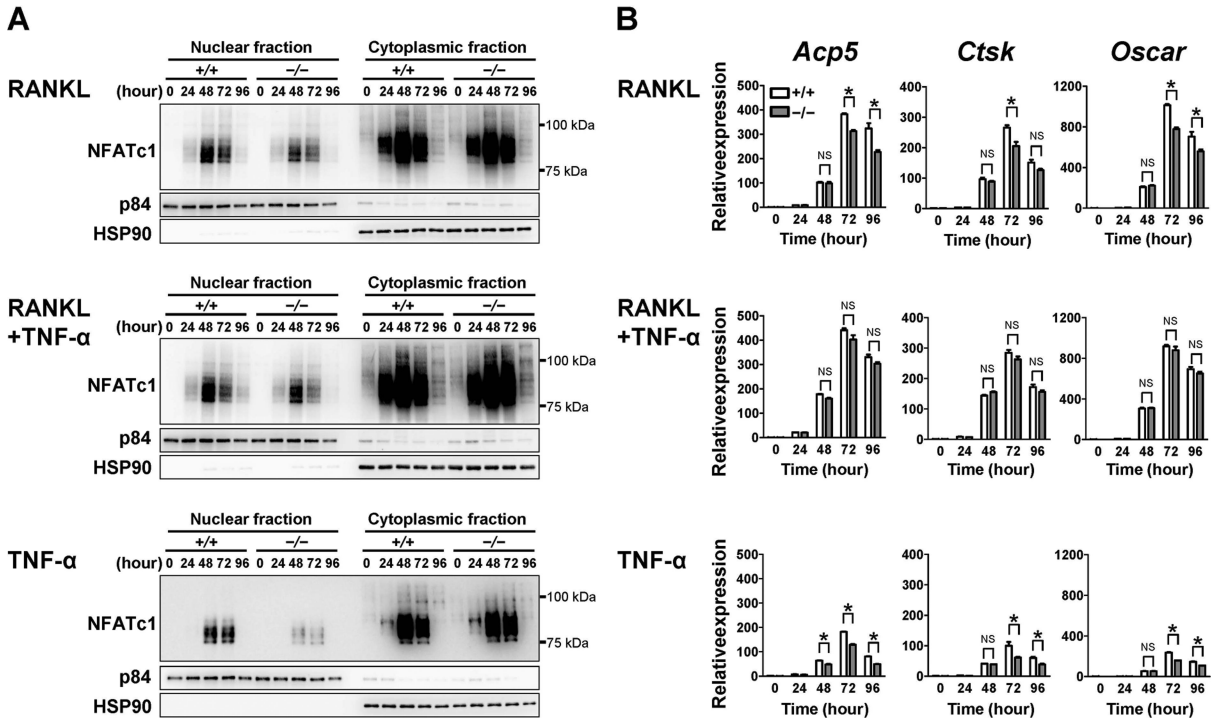

Figure 4.

Decreased NFATc1 nuclear localization in TNF-α-stimulated Sh3bp2$^{-/-}$ bone marrow-derived macrophages. **A–B**, BMMs were stimulated with RANKL alone (50 ng/ml), the combination of RANKL (50 ng/ml) and TNF-α (100 ng/ml), and TNF-α alone (100 ng/ml) in the presence of M-CSF (25 ng/ml). **A**, Western blot analysis of NFATc1. Nuclear and cytoplasmic protein samples were isolated at indicated time points after stimulation. Nuclear matrix protein p84 (p84) and heat shock protein 90 (HSP90) were used as loading controls. **B**, qPCR analysis for *Acp5*, *Ctsk*, and *Oscar* gene expressions. mRNA expression levels relative to *Hprt* were calculated and normalized to the average expression levels of *Sh3bp2*$^{+/+}$ BMMs at 0 hour. Values are presented as the mean ± SEM. +/+ = *Sh3bp2*$^{+/+}$; −/− = *Sh3bp2*$^{-/-}$. * = $P < 0.05$.

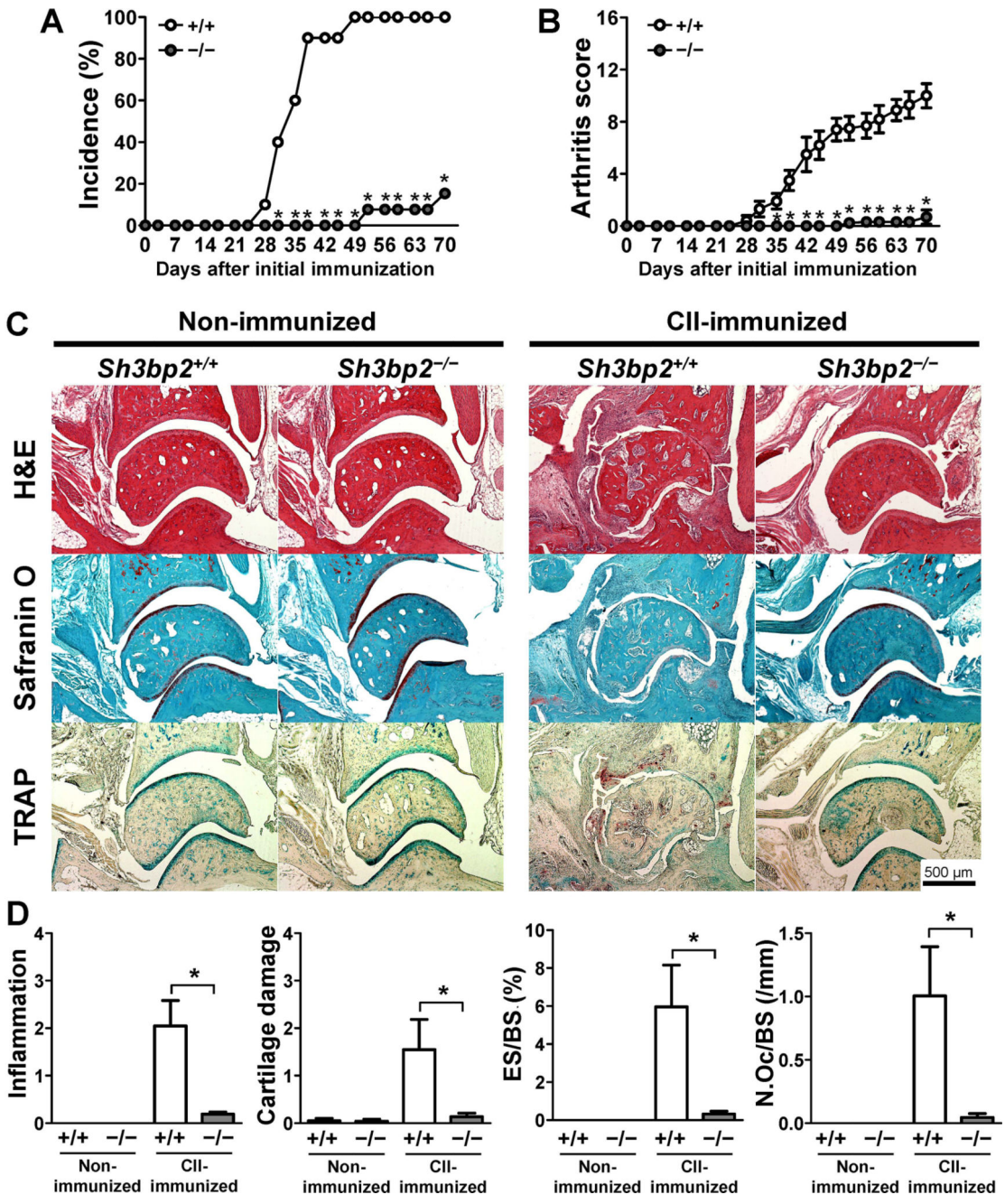

Figure 5.

Lower incidence and severity of arthritis in Sh3bp2$^{-/-}$ mice in the CIA model. Nine-week-old *Sh3bp2*$^{+/+}$ (*n* = 10) and *Sh3bp2*$^{-/-}$ (*n* = 13) male mice were immunized with chick type II collagen (CII) in complete Freund's adjuvant on day 0, followed by boost injection at day 21. Swelling of the paws was evaluated until day 70. **A**, Incidence of arthritis. **B**, Arthritis score of CII-immunized mice. *Sh3bp2*$^{+/+}$ (*n* = 10) and *Sh3bp2*$^{-/-}$ (*n* = 13) mice. **C**–**D,** Left hindlimbs were collected from CII-immunized *Sh3bp2*$^{+/+}$ (*n* = 10) and *Sh3bp2*$^{-/-}$ (*n* = 13) male mice at day 70. Age-matched non-immunized *Sh3bp2*$^{+/+}$ (*n* = 7) and *Sh3bp2*$^{-/-}$ (*n* = 7) mice were used as controls. **C**, Representative staining images of the ankle joint tissues.

Ankle joint sections were stained with H&E, Safranin O, and TRAP. Original magnification, 40X. **D**, Histological score of inflammation and cartilage damage and histomorphometric analysis of talar bones. Bone erosion on the surface of the talus was traced, and attached osteoclasts were counted. ES/BS and N.Oc/BS of the talus were determined. Values are presented as the mean ± SEM. +/+ =*Sh3bp2*$^{+/+}$; −/− = *Sh3bp2*$^{-/-}$. * = $P < 0.05$.

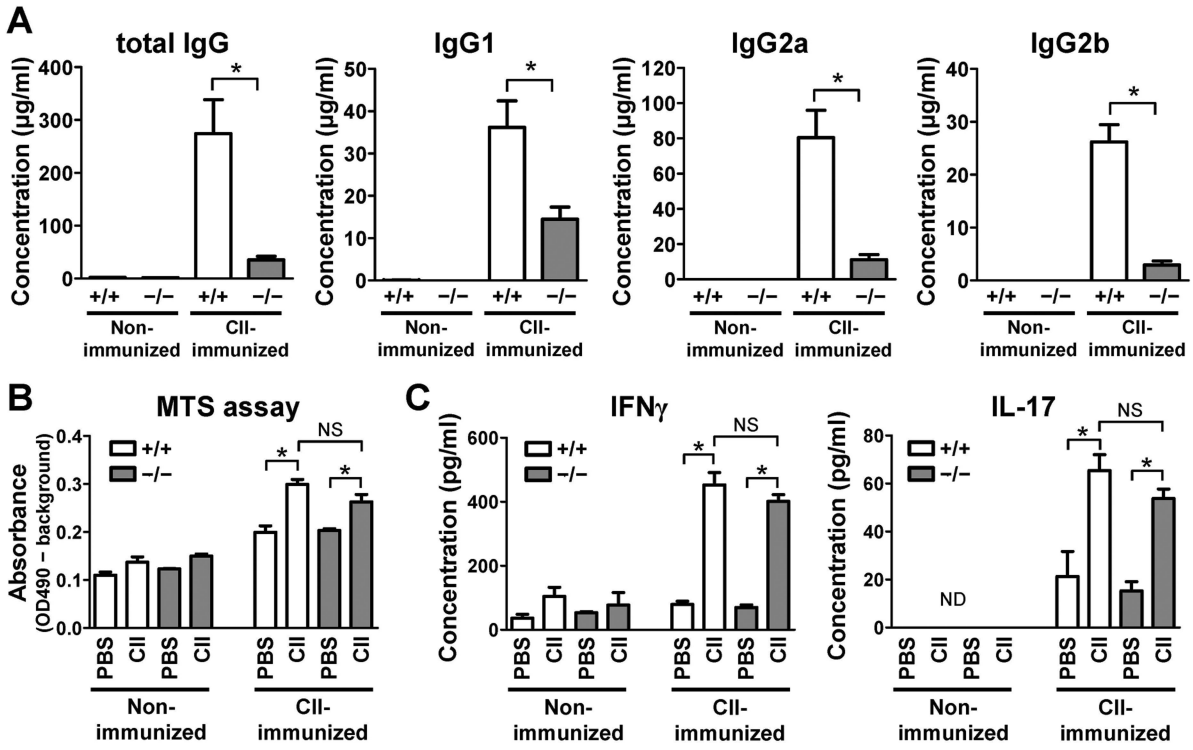

Figure 6.

Impaired anti-mouse CII antibody production in Sh3bp2$^{-/-}$ mice. **A**, Serum samples were collected from CII-immunized *Sh3bp2*$^{+/+}$ (n = 10) and *Sh3bp2*$^{-/-}$ (n = 13) male mice at day 70. Serum samples from age-matched non-immunized *Sh3bp2*$^{+/+}$ (n = 7) and *Sh3bp2*$^{-/-}$ (n = 7) male mice were used as controls. Total IgG, IgG1, IgG2a, and IgG2b against mouse CII were measured by ELISA. **B**–**C**, Inguinal lymph nodes were isolated from CII-immunized mice at 10 days after the immunization with chick CII and from age-matched non-immunized mice as controls. Lymph node cells (4×10^5 cells/well) were stimulated with chick CII (50 μg/ml) for 72 hours. Proliferation of the cells was determined by a colorimetric assay using MTS reagent (**B**). Levels of IFNγ and IL-17 in culture supernatant were measured by ELISA (**C**). The lower limit of detection is 10 pg/ml. Values are presented as the mean ± SEM. +/+ = *Sh3bp2*$^{+/+}$; −/− = *Sh3bp2*$^{-/-}$. * = $P < 0.05$; NS = not significant; ND = not detectable.